

Thermal transport of fractionalized antiferromagnetic and field-induced states in the Kitaev material $\text{Na}_2\text{Co}_2\text{TeO}_6$

Shuangkui Guang,^{1,*} Na Li,^{2,*} Rui Leonard Luo,³ Qing Huang,⁴ Yiyuan Wang,⁵ Xiaoyue Yue,⁵ Ke Xia,¹ Qiuju Li,⁶ Xia Zhao,⁷ Gang Chen,³ Haidong Zhou,^{4,†} and Xuefeng Sun,^{3,1,5,‡}

¹*Department of Physics and Key Laboratory of Strongly-Coupled Quantum Matter Physics (CAS), University of Science and Technology of China, Hefei, Anhui 230026, People's Republic of China*

²*Hefei National Research Center for Physical Sciences at Microscale,*

University of Science and Technology of China, Hefei, Anhui 230026, People's Republic of China

³*Department of Physics and HKU-UCAS Joint Institute for Theoretical and Computational Physics at Hong Kong, The University of Hong Kong, Hong Kong, People's Republic of China*

⁴*Department of Physics and Astronomy, University of Tennessee, Knoxville, Tennessee 37996-1200, USA*

⁵*Institute of Physical Science and Information Technology, Anhui University, Hefei, Anhui 230601, People's Republic of China*

⁶*School of Physics and Optoelectronic Engineering, Anhui University, Hefei, Anhui 230601, People's Republic of China*

⁷*School of Physical Sciences, University of Science and Technology of China, Hefei, Anhui 230026, People's Republic of China*



(Received 16 November 2022; revised 12 April 2023; accepted 25 April 2023; published 10 May 2023)

We report an in-plane thermal transport study of the honeycomb Kitaev material $\text{Na}_2\text{Co}_2\text{TeO}_6$ at sub-Kelvin temperatures. In zero magnetic field, the $\kappa(T)$ displays a rather weak T dependence but has a nonzero residual term κ_0/T , indicating strong phonon scattering by magnetic excitation and the possibility of itinerant spinonlike excitations coexisting with an antiferromagnetic order below 27 K. We propose the zero-field ground state is a fractionalized antiferromagnetic (AF*) state with both magnetic order and fractionalized excitations. With both the heat current and magnetic field along the a^* (Co-Co bond) direction, the $\kappa_{a^*}(B)$ exhibits two sharp minima at 7.5 and 10 T, which confirms the phase boundaries of the reported field-induced intermediate state. No such intermediate phase was found in the $\kappa_a(B)$ for the current and field along the a (zigzag chain) direction. Finally, $\text{Na}_2\text{Co}_2\text{TeO}_6$ displays a strongly anisotropic magneto-thermal conductivity since the in-plane (out-of-plane) field strongly enhances (suppresses) κ_{a^*} and κ_a .

DOI: [10.1103/PhysRevB.107.184423](https://doi.org/10.1103/PhysRevB.107.184423)

I. INTRODUCTION

The Mott insulators with substantial spin-orbit coupling are promising candidates to realize novel and exotic quantum phases that can be difficult to achieve without the spin-orbit coupling [1]. These physics are particularly relevant for many $4d/5d$ transition metal oxides and even for the $4f$ rare-earth compounds. Interesting quantum phases such as quantum spin ice, magnetic multipolar orders, quantum spin liquids, topological Mott insulator, etc., have been proposed and discussed among these materials [2–8]. In comparison with these heavy ions, the spin-orbit coupling of the $3d$ transition metal ions is usually much weaker and thus, much less discussed. Most often, the spin-orbit coupling is responsible for the generation of weak anisotropies such as the Dzyaloshinskii-Moriya interaction and the single-ion spin anisotropy, and can be neglected in most cases [9]. In certain cases, however, the spin-orbit coupling could play an interesting and sometimes indispensable role in the $3d$ transition metal compounds. For Mott insulators, this scenario was suggested to

occur for the partially filled t_{2g} shell of the Ni^{2+} ions in the tetrahedral crystal field environment [10] and the Co^{2+} ions in the octahedral crystal field environment [11–13], where the spin-orbit coupling is active in the linear order, and the partially filled e_g shell of the Fe^{2+} ions in the tetrahedral crystal field environment [14,15], and the spin-orbit coupling is active in the quadratic order. Due to the spin-orbit entanglement and the effective $J = 1/2$ local moments, the Co-based honeycomb lattice antiferromagnets, $\text{Na}_2\text{Co}_2\text{TeO}_6$, $\text{Na}_3\text{Co}_2\text{SbO}_6$, and $\text{BaCo}_2(\text{AsO}_4)_2$, were proposed as candidate Kitaev materials beyond the original $4d/5d$ contexts [11–13,16,17].

Compared with the $4d/5d$ compounds like $A_2\text{IrO}_3$ ($A = \text{Na, Li}$) and $\alpha\text{-RuCl}_3$, the high-spin $3d^7$ configuration of the Co ions can induce a cancellation mechanism for the nearest-neighbor Heisenberg interactions [11–13]. $\text{Na}_2\text{Co}_2\text{TeO}_6$ does not have the monoclinic distortion of the $4d/5d$ Kitaev materials [18–20]. Like $\alpha\text{-RuCl}_3$, $\text{Na}_2\text{Co}_2\text{TeO}_6$ also develops an antiferromagnetic (AF) order at low temperatures below $T_N \sim 27$ K. This magnetic order was suggested to be either a zigzag [18,19] or three- q [21,22] AF order. Moreover, the in-plane magnetic field can induce a successive phase transition, and an intermediate magnetic state exists between the ground-state AF order and the spin polarized state [23,24].

*These authors contributed equally to this work.

†hzhou10@utk.edu

‡xfsun@ustc.edu.cn

Thermal transport measurements were suggested to be crucial to characterize the properties of the low-energy excitations of various quantum magnets and have been used to probe the spinon excitations in various spin-liquid candidate materials. At present, only a few quantum spin liquid candidates exhibit the residual thermal conductivity at zero temperature limit, κ_0/T , a fingerprint of the itinerant fermionic excitations [25–28]. Whereas, some controversial results of the absence of κ_0/T have also been reported for these candidate materials [29–32]. The previous ultralow-temperature thermal conductivity experiments on α -RuCl₃ indicated that there is no spinon transport in either zero field or high magnetic field [33]. The observations of the quantum oscillation in thermal conductivity and the half quantized thermal Hall conductivity in the proposed field-induced spin liquid of α -RuCl₃, however, support the exotic spinonlike excitations [34–36]. In contrast, Na₂Co₂TeO₆ was reported to have the dominant phononic thermal conductivity with a significant spin-phonon scattering at the ordinary low temperatures [37], and the thermal Hall effect measurements at not very low temperatures revealed the magnon heat transport [38–40]. In this work, we investigate the thermal conductivity (κ) of Na₂Co₂TeO₆ at ultralow temperatures and provide some understanding of the low-energy excitations and the field-driven magnetic phases.

II. EXPERIMENTS

High-quality single crystals of Na₂Co₂TeO₆ were synthesized by a conventional solid reaction as previous reports [24,41]. A polycrystalline sample was mixed with the flux of Na₂O and TeO₂ in a molar ratio of 1: 0.5: 2 and gradually heated to 900 °C at 3 °C/min in the air after grinding. The sample was retained at 900 °C for 30 hours and was cooled to 500 °C at the rate of 3 °C/h. The furnace was then shut down to cool to room temperature. The as-grown single crystals are thin plates with size up to 10 × 5 × 0.06 mm³. The orientation of the crystals was confirmed by an x-ray Laue back diffraction measurement. Thermal conductivity was measured by using a “one heater, two thermometers” technique in a ³He / ⁴He dilution refrigerator at 70 mK–1.2 K, equipped with a 14 T superconducting magnet [27,28]. Two rectangular shaped samples were cut from as-grown crystals. Sample A has the dimension of 4.92 × 1.56 × 0.051 mm³ with the length along the a axis (zigzag chain), while sample B has the dimension of 5.17 × 1.56 × 0.056 mm³ with the length along the a^* axis (Co-Co bond). The heat current was applied along the longest dimension of samples. The magnetic fields were applied along either the longest dimension of the samples (the a or a^* axis) or the shortest one (the c axis). The temperature gradients were measured by two *in situ* calibrated RuO₂ thermometers. The field dependence of κ was measured with zero-field cooling from 30 K (above T_N) to the fixed temperatures.

III. RESULTS AND DISCUSSIONS

In Fig. 1(a), we depict the temperature dependence of κ_a and κ_{a^*} , measured in zero magnetic field and with heat current along the a axis (the zigzag direction, sample A) and

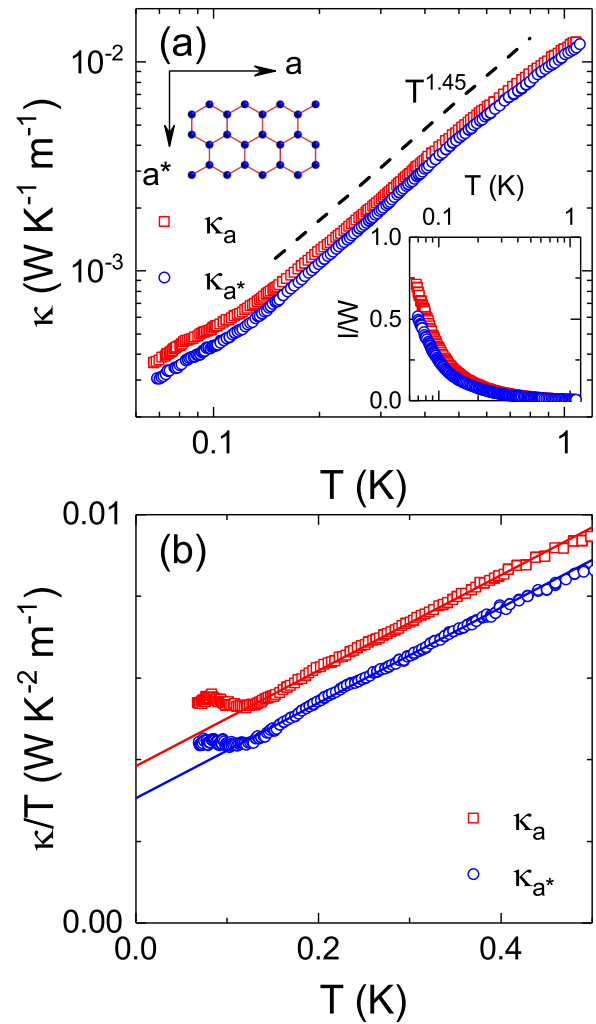


FIG. 1. (a) Temperature dependence of the thermal conductivity κ_a and κ_{a^*} , measured in zero magnetic field and with heat current along the a axis (the zigzag direction) and the a^* axis (the Co-Co bond direction), respectively. The dashed line indicates a $T^{1.45}$ -dependence of κ in temperature range of 150–600 mK. The insets of (a) demonstrate the direction of a and a^* axes, and the ratio of estimated phonon mean free path to the averaged sample width. (b) Low-temperature data plotted with κ/T vs T . The solid lines are linear fittings to $\kappa/T = \kappa_0/T + bT$ for $120 < T < 400$ mK.

the a^* axis (the Co-Co bond direction, sample B), respectively. It is known that Na₂Co₂TeO₆ enters a zigzag [18,19] or triple- q [21,22] AF order below $T_N \sim 27$ K, followed by two possible spin reorientation transitions around 16 K and 6 K [18,20,24,42]. In present measurements, the temperature range is much lower than T_N . The magnitudes of κ_a and κ_{a^*} are comparable, indicating nearly isotropic heat transport in the honeycomb layer. The $\kappa(T)$ shows a roughly $T^{1.45}$ behavior at 150–600 mK, as shown in Fig. 1(a), which strongly deviates from the standard T^3 behavior for either phonon or magnon thermal conductivity at very low temperatures [43]. In addition, assuming that the thermal conductivity is purely phononic, the phonon mean free path can be calculated [44]. The inset of Fig. 1 shows the ratios of the phonon mean free path to the averaged sample width, which are smaller than one

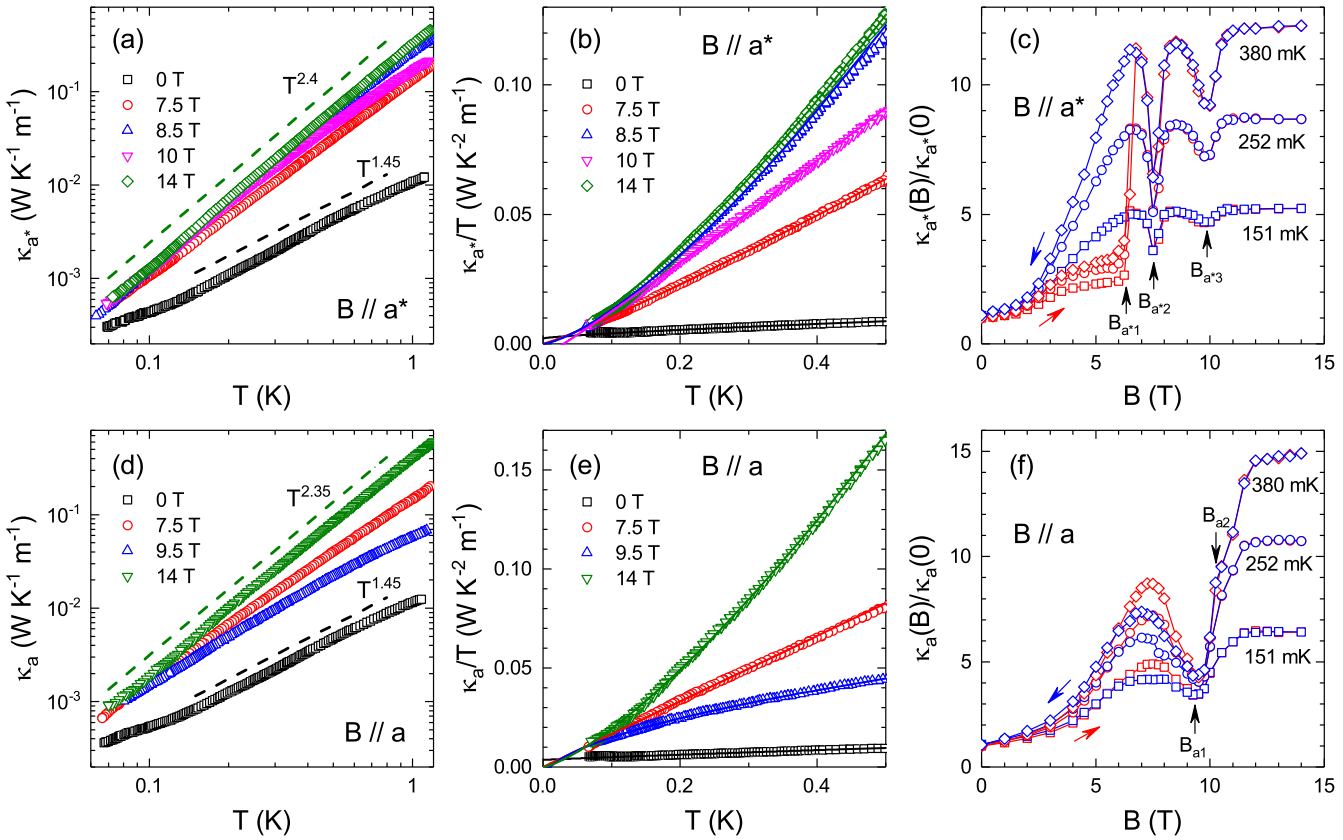


FIG. 2. (a) Temperature dependence of κ_{a*} for different magnetic fields along the a^* axis. The dashed lines indicate the $T^{1.45}$ and $T^{2.4}$ dependence of κ_{a*} in 0 and 14 T. (b) Low-temperature data plotted with κ_{a*}/T vs T . The solid lines are fittings to $\kappa_{a*}/T = \kappa_0/T + bT^{\alpha-1}$ for $T < 400$ mK with $\alpha = 2.11, 2.39, 2.06$, and 2.42 for 7.5, 8.5, 10, and 14 T, respectively. (c) κ_{a*} as a function of magnetic field ($\parallel a^*$) at 151, 252, and 380 mK. The red and blue symbols indicate the measurements with increasing and decreasing field, respectively. The black arrows indicate three critical fields B_{a*1} , B_{a*2} , and B_{a*3} . (d) Temperature dependence of κ_a for different magnetic fields along the a axis. The dashed lines indicate the $T^{1.45}$ and $T^{2.35}$ dependence of κ_a in 0 and 14 T. (e) Low-temperature data plotted with κ_a/T vs T . The solid lines are fittings to $\kappa_a/T = \kappa_0/T + bT^{\alpha-1}$ for $T < 400$ mK with $\alpha = 1.99, 1.55$, and 2.34 for 7.5, 9.5, and 14 T, respectively. (f) κ_a as a function of magnetic field ($\parallel a$) at 151, 252, and 380 mK. The red and blue symbols indicate the data measured with increasing and decreasing field, respectively. The black arrows indicate two critical fields B_{a1} and B_{a2} .

and indicate the existence of microscopic phonon scattering effect at such low temperatures. Apparently, there is strong scattering between the phonons and magnetic excitations in zero field.

The temperature dependence of κ at ultralow temperatures is somewhat different. Figure 1(b) shows the ultralow temperature data plotted with κ/T vs T , which can be linearly fitted in a rather broad temperature range of 120–400 mK, with a small but nonzero residual term κ_0/T of 0.0038 and 0.0030 W K⁻² m⁻¹ for κ_a and κ_{a*} , respectively. In quantum magnets, the κ at ultralow temperatures can often be fitted to $\kappa/T = \kappa_0/T + bT^{\alpha-1}$, in which the two terms represent contributions from the itinerant fermionic magnetic excitations and phonons, respectively [25–28]. The power α can be equal to three under the boundary scattering limit, or smaller due to the phonon reflection at the sample surfaces or the spin-phonon scattering. We further note that the κ/T is nearly T independent at $T < 120$ mK and points to larger residual terms, which could be due to the recovery of κ by the itinerant excitations at extremely low temperatures. Note that a recent ultralow-temperature heat transport study by Takeda *et al.* [40] revealed even larger κ_0/T for κ_a (See the Supplemental

Material [45]). It is very surprising to observe such a nonzero residual term for $\text{Na}_2\text{Co}_2\text{TeO}_6$ since it has an AF order at zero field. We interpret this result by proposing the ground state of $\text{Na}_2\text{Co}_2\text{TeO}_6$ as a fractionalized antiferromagnet (AF*), where there exist both AF order and the fractionalized spinon-like excitation in the system. Such a state was actually firstly proposed theoretically in the context of high-temperature superconducting cuprates, whose relevance is still unclear [46]. The presence of a residual thermal conductance indicates the presence of a Fermi surface or Dirac spectra of the fractionalized particles. Based on the inelastic neutron scattering results that have linearly dispersive spectral weights around the M and Γ points [21], it is more natural to expect Dirac spectra for the fractionalized particles and the M (Γ) point scattering corresponds to the inter- (intra-) Dirac cone scattering. In fact, recent theoretical progress that worked on a realistic model for $\text{Na}_2\text{Co}_2\text{TeO}_6$ also proposed such a fractionalized antiferromagnetic state from both numerical and theoretical analysis [47].

Figure 2(a) shows the temperature dependence of κ_{a*} in different magnetic fields along the a^* axis. The $\kappa_{a*}(T)$ in magnetic fields displays larger values and stronger temper-

ture dependence; for example, at 14 T it shows a rough $T^{2.4}$ behavior, which is rather close to the T^3 law. This can be due to the magnetic field suppressing magnetic excitations and weakening the spin-phonon scattering. Figure 2(b) shows the same data plotted with κ_{a*}/T vs T . For different magnetic fields along the a^* axis, the $\kappa/T = \kappa_0/T + bT^{\alpha-1}$ fitting gives zero or small negative value of κ_0/T , which means no residual term in magnetic fields. Similar results were obtained for κ_a with magnetic field along the a axis, as shown in Figs. 2(d) and 2(e). Figure 2(c) shows the magnetic field dependence of κ_{a*} for $B \parallel a^*$. With increasing field, the κ_{a*} firstly increases gradually and shows a sharp increase at $B_{a*1} \sim 6.25$ T; subsequently, the $\kappa_{a*}(B)$ exhibits two minima at $B_{a*2} \sim 7.5$ T and $B_{a*3} \sim 10$ T before getting saturation. The κ_{a*} with decreasing field is much larger than those with increasing field at $B < B_{a*1}$, displaying a large and broad hysteresis.

The rather sharp minima of $\kappa_{a*}(B)$ at B_{a*2} and B_{a*3} clearly indicate two magnetic transitions since a minimum of thermal conductivity most likely results from the strong scattering of phonons by magnetic fluctuations at the critical point [27,38,48–50]. The recent inelastic neutron scattering measurements with $B \parallel a^*$ revealed a field-induced intermediate magnetic state with partially polarized spins between 7.5 and 10 T [51], which correspond to the B_{a*2} and B_{a*3} . For this state, the signature is the coexistence of magnon and the gapless continuum mode that possibly represents spinon [51]. Our thermal conductivity data here further validates the phase boundaries of this phase. The disappearance of hysteresis in this intermediate phase also supports its spin disordered nature.

The observed hysteresis of $\kappa_{a*}(B)$ is unusual. Based on the previous magnetization study, the B_{a*1} corresponds to a first-order transition associated with the field-induced reversal of canting moments [23,24]. Although the first-order magnetic transition can induce a hysteresis in the $\kappa(B)$ curve [49,52,53], it usually occurs in a rather narrow region near the transition field. The present hysteresis is so broad that it extends from B_{a*1} to zero field. However, this broad hysteresis at very low temperatures may be directly related to the magnetization hysteresis, which is clearly broadened with lowering temperature (from 10 to 2 K) [24].

Figure 2(f) shows the magnetic field dependence of κ_a for $B \parallel a$. With increasing field, the κ_a firstly increases and arrives a maximum at ~ 7.5 T, and then decreases and reaches a minimum at ~ 9.75 T, which is marked as B_{a1} in the figure. This critical field is rather close to the spin polarization transition for $B \parallel a$. Above B_{a1} , the κ_a quickly increases and finally saturates in the polarized state. It is notable that there is a kink or slope change in the $\kappa_a(B)$ at 10.25–10.5 T, which is marked as B_{a2} . This anomaly is unexpected since the spins should be already polarized. There is an obvious hysteresis between the increasing and decreasing field data for $B < B_{a1}$.

The comparison between $\kappa_{a*}(B)$ and $\kappa_a(B)$ clearly shows that the field-induced intermediate phase only exists while $B \parallel a^*$. The previous magnetization measurements did not show any hysteresis for $B \parallel a$ [23,24], so the hysteresis in $\kappa_a(B)$ is not simply due to the possible irreversible magnetization behavior. Furthermore, this hysteresis is rather odd since the relative magnitude of κ is different at the intermediate fields

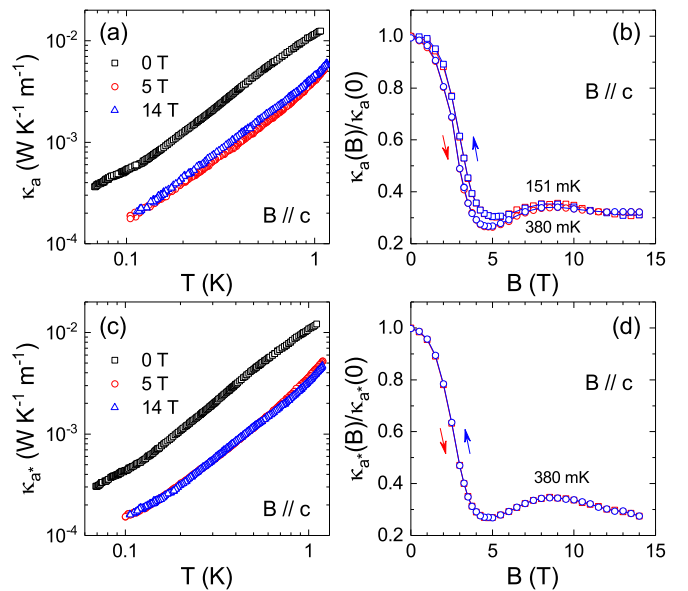


FIG. 3. (a) Temperature dependence of κ with the heat current and magnetic field along the a axis and the c axis, respectively. (b) Magnetic field dependence of κ_a at 151 and 380 mK, the red and blue symbols indicate the data for increasing and decreasing field, respectively. (c) Temperature dependence of κ with the heat current and magnetic field along the a^* axis and the c axis, respectively. (d) Magnetic field dependence of κ_{a*} at 380 mK, the red and blue symbols indicate the data for increasing and decreasing field, respectively.

and low fields (< 5.5 T). It is likely to be associated with some magnetic domain structures that can scatter phonons [44,54]. If these domains are of the AF type, they do not induce irreversible magnetization.

Finally, we checked the in-plane thermal conductivity measured with $B \parallel c$. Figure 3(a) shows the temperature dependence of κ_a with $B \parallel c$. In either 5 or 14 T, the κ_a displays similar temperature dependence to that of the zero-field data while the magnitude of κ_a is much smaller in these fields. Figure 3(b) shows the field dependence of κ_a for $B \parallel c$ at 151 and 380 mK. With increasing field, the κ_a decreases quickly to reach a minimum around 5 T and displays a weak field dependence up to 14 T, with a small and broad peak at ~ 8 T. In addition, the $\kappa_a(B)$ curves for $B \parallel c$ have no hysteresis between the increasing and decreasing field data. Figures 3(c) and 3(d) show the data for the same measurements with the heat current and magnetic field along the a^* axis and the c axis, respectively. Both the temperature dependence and field dependence are nearly the same between κ_a and κ_{a*} . That is, the c -axis field induces isotropic effect on the a -axis and a^* -axis heat transport properties. The field dependence of κ for $B \parallel c$ can be due to more significant magnon-phonon scattering in the c -axis fields. Whereas, the minimum at $\kappa(B)$ is likely due to two competitive contributions of magnons induced by magnetic fields. With increasing field, the magnon gap will shrink and the magnon excitations will be populated; thus, the magnon transport can enhance the κ while the stronger magnon-phonon scattering can suppress the κ . Since the magnetization data did not show any signature of spin structure transitions at low fields for $B \parallel c$ [23,24], the

valley of $\kappa(B)$ at low fields is likely due to the competition of these two effects. It is notable the $\kappa(B)$ with $B \parallel c$ do not show hysteresis with sweeping field up and down. It should be pointed out that a recent heat transport study revealed that there is a clear hysteresis in $\kappa(B)$ for $B \parallel c$ at temperatures down to 8 K [39], which was ascribed to the small ferromagnetic moment along the c axis [24]. However, the present ultralow-temperature data do not exhibit hysteresis in $\kappa(B)$. In addition, our previous $\kappa(B)$ data at 0.36–1.95 K consistently did not show hysteresis [38]. Therefore, for $B \parallel c$ the hysteresis of $\kappa(B)$ appears at high temperatures.

It is obvious that the in-plane thermal conductivity of $\text{Na}_2\text{Co}_2\text{TeO}_6$ is enhanced by the in-plane field but suppressed by the out-of-plane field. Such anisotropic magneto-thermal conductivity is rather rare in magnetic materials, in which the magnetic fields in different directions usually affect the thermal conductivity in the similar way [27,28,55]. To our knowledge, only $\text{NiCl}_2\text{-4SC}(\text{NH}_2)_2$, a spin-1 chain system, was found to exhibit anisotropic magneto-thermal conductivity, in which the magnetic field along (perpendicular) the spin chains enhances (suppresses) the thermal conductivity [56]. This anisotropy is related to the field induced magnon Bose-Einstein condensation state along the spin-chain direction. However, the present $\text{Na}_2\text{Co}_2\text{TeO}_6$ result must have a different mechanism, and we think this is due to the combined effects of the anisotropic magnetic interaction and the specific magnetic structures. Moreover, the $\kappa_{a*}(B)$ and $\kappa_a(B)$ are obviously different, too. First, the $\kappa_{a*}(B)$ shows the field-induced intermediate magnetic state but $\kappa_a(B)$ does not. Second, within the hysteresis, the $\kappa_{a*}(B)$ is larger with the decreasing

field for $B \parallel a*$ while the $\kappa_a(B)$ is larger with the increasing field for $B \parallel a$. All these differences indicate that in the ab plane, the exchange interactions along the $a*$ and a directions are different from each other, which should be accounted for in future studies.

IV. SUMMARY

Our ultralow-temperature thermal conductivity data of $\text{Na}_2\text{Co}_2\text{TeO}_6$ suggests the existence of itinerant fermionic magnetic excitations in the zero magnetic field that is interpreted from the fractionalized antiferromagnet. We further show the existence of the intermediate magnetic state for $B \parallel a*$ from the magnetic field dependence of κ . Moreover, our data show that $\text{Na}_2\text{Co}_2\text{TeO}_6$ is a rare magnet exhibiting strong anisotropic magneto-thermal conductivity. Such complex thermal conductivity behaviors reflect the unique exchange interactions in $\text{Na}_2\text{Co}_2\text{TeO}_6$, which call for further studies to be clarified.

ACKNOWLEDGMENTS

We acknowledge very useful discussion with Yuan Li. This work was supported by the National Natural Science Foundation of China (Grants No. 12274388, No. 12174361, No. 12104011, No. 12104010, No. U1832209, and No. 11874336), the Nature Science Foundation of Anhui Province (Grants No. 1908085MA09 and No. 2108085QA22), and Hong Kong CRF. The work at the University of Tennessee was supported by the NSF with Grant No. NSF-DMR-2003117.

[1] W. Witczak-Krempa, G. Chen, Y. B. Kim, and L. Balents, Correlated Quantum Phenomena in the Strong Spin-Orbit Regime, *Annu. Rev. Condens. Matter Phys.* **5**, 57 (2014).

[2] Y. Zhou, K. Kanoda, and T. K. Ng, Quantum spin liquid states, *Rev. Mod. Phys.* **89**, 025003 (2017).

[3] L. Savary and L. Balents, Quantum spin liquids: A review, *Rep. Prog. Phys.* **80**, 016502 (2017).

[4] M. J. P. Gingras and P. A. McClarty, Quantum spin ice: A search for gapless quantum spin liquids in pyrochlore magnets, *Rep. Prog. Phys.* **77**, 056501 (2014).

[5] D. Pesin and L. Balents, Mott physics and band topology in materials with strong spin-orbit interaction, *Nat. Phys.* **6**, 376 (2010).

[6] C. Liu, Y.-D. Li, and G. Chen, Selective measurements of intertwined multipolar orders: Non-Kramers doublets on a triangular lattice, *Phys. Rev. B* **98**, 045119 (2018).

[7] D. Hirai, H. Sagayama, S. Gao, H. Ohsumi, G. Chen, T. H. Arima, and Z. Hiroi, Detection of multipolar orders in the spin-orbit-coupled 5d Mott insulator $\text{Ba}_2\text{MgReO}_6$, *Phys. Rev. Res.* **2**, 022063(R) (2020).

[8] Y.-D. Li, X. Wang, and G. Chen, Hidden multipolar orders of dipole-octupole doublets on a triangular lattice, *Phys. Rev. B* **94**, 201114(R) (2016).

[9] S. Maekawa, T. Tohyama, S. E. Barnes, S. Ishihara, W. Koshiba, and G. Khaliullin, *Physics of Transition Metal Oxides*, Springer Series in Solid State Sciences, Vol. 144 (Springer-Verlag Berlin Heidelberg, 2004).

[10] F.-Y. Li and G. Chen, Spin-orbital entanglement in d^8 Mott insulators: Possible excitonic magnetism in diamond lattice antiferromagnets, *Phys. Rev. B* **100**, 045103 (2019).

[11] H. Liu and G. Khaliullin, Pseudospin exchange interactions in d^7 cobalt compounds: Possible realization of the Kitaev model, *Phys. Rev. B* **97**, 014407 (2018).

[12] R. Sano, Y. Kato, and Y. Motome, Kitaev-Heisenberg Hamiltonian for high-spin d^7 Mott insulators, *Phys. Rev. B* **97**, 014408 (2018).

[13] H. Liu, J. Chaloupka, and G. Khaliullin, Kitaev Spin Liquid in 3d Transition Metal Compounds, *Phys. Rev. Lett.* **125**, 047201 (2020).

[14] G. Chen, L. Balents, and A. P. Schnyder, Spin-Orbital Singlet and Quantum Critical Point on the Diamond Lattice: FeSc_2S_4 , *Phys. Rev. Lett.* **102**, 096406 (2009).

[15] G. Chen, A. P. Schnyder, and L. Balents, Excitation spectrum and magnetic field effects in a quantum critical spin-orbital system: The case of FeSc_2S_4 , *Phys. Rev. B* **80**, 224409 (2009).

[16] R. Zhong, T. Gao, N. P. Ong, and R. J. Cava, Weak-field induced nonmagnetic state in a Co-based honeycomb, *Sci. Adv.* **6**, eaay6953 (2020).

[17] A. Kitaev, Anyons in an exactly solved model and beyond, *Ann. Phys.* **321**, 2 (2006).

[18] E. Lefrançois, M. Songvilay, J. Robert, G. Nataf, E. Jordan, L. Chaix, C. V. Colin, P. Lejay, A. Hadj-Azzem, R. Ballou, and V. Simonet, Magnetic properties of the honeycomb oxide $\text{Na}_2\text{Co}_2\text{TeO}_6$, *Phys. Rev. B* **94**, 214416 (2016).

[19] A. K. Bera, S. M. Yusuf, A. Kumar, and C. Ritter, Ziazag anti-ferromagnetic ground state with anisotropic correlation lengths in the quasi-two-dimensional honeycomb lattice compound $\text{Na}_2\text{Co}_2\text{TeO}_6$, *Phys. Rev. B* **95**, 094424 (2017).

[20] L. Viciu, Q. Huang, E. Morosan, H. Zandbergen, N. Greenbaum, T. McQueen, and R. Cava, Structure and basic magnetic properties of the honeycomb lattice compounds $\text{Na}_2\text{Co}_2\text{TeO}_6$ and $\text{Na}_3\text{Co}_2\text{SbO}_6$, *J. Solid State Chem.* **180**, 1060 (2007).

[21] W. Chen, X. Li, Z. Hu, Z. Hu, L. Yue, R. Sutarto, F. He, K. Iida, K. Kamazawa, W. Yu, X. Lin, and Y. Li, Spin-orbit phase behavior of $\text{Na}_2\text{Co}_2\text{TeO}_6$ at low temperatures, *Phys. Rev. B* **103**, L180404 (2021).

[22] C. H. Lee, S. Lee, Y. S. Chio, Z. H. Jang, R. Kalaivanan, R. Sankar, and K.-Y. Chio, Multistage development of anisotropic magnetic correlations in the Co-based honeycomb lattice $\text{Na}_2\text{Co}_2\text{TeO}_6$, *Phys. Rev. B* **103**, 214447 (2021).

[23] G. Lin, J. Jeong, C. Kim, Y. Wang, Q. Huang, T. Masuda, S. Asai, S. Itoh, G. Günther, M. Russina, Z. Lu, J. Sheng, L. Wang, J. Wang, G. Wang, Q. Ren, C. Xi, W. Tong, L. Ling, Z. Liu *et al.*, Field-induced quantum spin disordered state in spin-1/2 honeycomb magnet $\text{Na}_2\text{Co}_2\text{TeO}_6$, *Nat. Commun.* **12**, 5559 (2021).

[24] W. Yao and Y. Li, Ferrimagnetism and anisotropic phase tunability by magnetic fields in $\text{Na}_2\text{Co}_2\text{TeO}_6$, *Phys. Rev. B* **101**, 085120 (2020).

[25] M. Yamashita, N. Nakata, Y. Senshu, M. Nagata, H. M. Yamamoto, R. Kato, T. Shibauchi, and Y. Matsuda, Highly Mobile Gapless Excitations in a Two-Dimensional Candidate Quantum Spin Liquid, *Science* **328**, 1246 (2010).

[26] H. Murayama, Y. Sato, T. Taniguchi, R. Kurihara, X. Z. Xing, W. Huang, S. Kasahara, Y. Kasahara, I. Kimchi, M. Yoshida, Y. Iwasa, Y. Mizukami, T. Shibauchi, M. Konczykowski, and Y. Matsuda, Effect of quenched disorder on the quantum spin liquid state of the triangular-lattice antiferromagnet $1T\text{-TaS}_2$, *Phys. Rev. Res.* **2**, 013099 (2020).

[27] N. Li, Q. Huang, X. Y. Yue, W. J. Chu, Q. Chen, E. S. Choi, X. Zhao, H. D. Zhou, and X. F. Sun, Possible itinerant excitations and quantum spin state transitions in the effective spin-1/2 triangular-lattice antiferromagnet $\text{Na}_2\text{BaCo}(\text{PO}_4)_2$, *Nat. Commun.* **11**, 4216 (2020).

[28] X. Rao, G. Hussain, Q. Huang, W. J. Chu, N. Li, X. Zhao, Z. Dun, E. S. Choi, T. Asaba, L. Chen, L. Li, X. Y. Yue, N. N. Wang, J.-G. Cheng, Y. H. Gao, Y. Shen, J. Zhao, G. Chen, H. D. Zhou, and X. F. Sun, Survival of itinerant excitations and quantum spin state transitions in YbMgGaO_4 with chemical disorder, *Nat. Commun.* **12**, 4949 (2021).

[29] P. Bourgeois-Hope, F. Laliberté, E. Lefrançois, G. Grissonnanche, S. René de Cotret, R. Gordon, S. Kitou, H. Sawa, H. Cui, R. Kato, L. Taillefer, and N. Doiron-Leyraud, Thermal Conductivity of the Quantum Spin Liquid Candidate $\text{EtMe}_3\text{Sb}[\text{Pd}(\text{dmit})_2]_2$: No Evidence of Mobile Gapless Excitations, *Phys. Rev. X* **9**, 041051 (2019).

[30] J. M. Ni, B. L. Pan, B. Q. Song, Y. Y. Huang, J. Y. Zeng, Y. J. Yu, E. J. Cheng, L. S. Wang, D. Z. Dai, R. Kato, and S. Y. Li, Absence of Magnetic Thermal Conductivity in the Quantum Spin Liquid Candidate $\text{EtMe}_3\text{Sb}[\text{Pd}(\text{dmit})_2]_2$, *Phys. Rev. Lett.* **123**, 247204 (2019).

[31] Y. J. Yu, Y. Xu, L. P. He, M. Kratochvílová, Y. Y. Huang, J. M. Ni, Lihai Wang, S.-W. Cheong, J.-G. Park, and S. Y. Li, Heat transport study of the spin liquid candidate $1T\text{-TaS}_2$, *Phys. Rev. B* **96**, 081111(R) (2017).

[32] Y. Xu, J. Zhang, Y. S. Li, Y. J. Yu, X. C. Hong, Q. M. Zhang, and S. Y. Li, Absence of Magnetic Thermal Conductivity in the Quantum Spin-Liquid Candidate YbMgGaO_4 , *Phys. Rev. Lett.* **117**, 267202 (2016).

[33] Y. J. Yu, Y. Xu, K. J. Ran, J. M. Ni, Y. Y. Huang, J. H. Wang, J. S. Wen, and S. Y. Li, Ultralow-Temperature Thermal Conductivity of the Kitaev Honeycomb Magnet $\alpha\text{-RuCl}_3$ across the Field-Induced Phase Transition, *Phys. Rev. Lett.* **120**, 067202 (2018).

[34] Y. Kasahara, T. Ohnishi, Y. Mizukami, O. Tanaka, S. Ma, K. Sugii, N. Kurita, H. Tanaka, J. Nasu, Y. Motome, T. Shibauchi, and Y. Matsuda, Majorana quantization and half-integer thermal quantum Hall effect in a Kitaev spin liquid, *Nature (London)* **559**, 227 (2018).

[35] P. Czajka, T. Gao, M. Hirschberger, P. Lampen-Kelley, A. Banerjee, J. Yan, D. G. Mandrus, S. E. Nagler, and N. P. Ong, Oscillations of the thermal conductivity in the spin-liquid state of $\alpha\text{-RuCl}_3$, *Nat. Phys.* **17**, 915 (2021).

[36] T. Yokoi, S. Ma, Y. Kasahara, S. Kasahara, T. Shibauchi, N. Kurita, H. Tanaka, J. Nasu, Y. Motome, C. Hickey, S. Trebst, and Y. Matsuda, Half-integer quantized anomalous thermal Hall effect in the Kitaev material candidate $\alpha\text{-RuCl}_3$, *Science* **373**, 568 (2021).

[37] X. Hong, M. Gillig, R. Henrich, W. Yao, V. Kocsis, A. R. Witte, T. Schreiner, D. Baumann, N. Pérez, A. U. B. Wolter, Y. Li, B. Büchner, and C. Hess, Strongly scattered phonon heat transport of the candidate Kitaev material $\text{Na}_2\text{Co}_2\text{TeO}_6$, *Phys. Rev. B* **104**, 144426 (2021).

[38] N. Li, R. R. Neumann, S. K. Guang, Q. Huang, J. Liu, K. Xia, X. Y. Yue, Y. Sun, Y. Y. Wang, Q. J. Li, Y. Jiang, J. Fang, Z. Jiang, X. Zhao, A. Mook, J. Henk, I. Mertig, H. D. Zhou, and X. F. Sun, Magnon-Polaron Driven Thermal Hall Effect in a Heisenberg-Kitaev Antiferromagnet, *arXiv:2201.11396* (2022).

[39] H. Yang, C. Kim, Y. Choi, J. H. Lee, G. Lin, J. Ma, M. Kratochvílová, P. Proschek, E.-G. Moon, K. H. Lee, Y. S. Oh, and J.-G. Park, Significant thermal Hall effect in the 3d cobalt Kitaev system $\text{Na}_2\text{Co}_2\text{TeO}_6$, *Phys. Rev. B* **106**, L081116 (2022).

[40] H. Takeda, J. Mai, M. Akazawa, K. Tamura, J. Yan, K. Moovendaran, K. Raju, R. Sankar, K.-Y. Choi, and M. Yamashita, Planar thermal Hall effects in the Kitaev spin liquid candidate $\text{Na}_2\text{Co}_2\text{TeO}_6$, *Phys. Rev. Res.* **4**, L042035 (2022).

[41] G. Xiao, Z. Xia, W. Zhang, X. Yue, S. Huang, X. Zhang, F. Yang, Y. Song, M. Wei, H. Deng, and D. Jiang, Crystal Growth and the Magnetic Properties of $\text{Na}_2\text{Co}_2\text{TeO}_6$ with Quasi-Two-Dimensional Honeycomb Lattice, *Cryst. Growth Des.* **19**, 2658 (2019).

[42] G. Xiao, Z. Xia, Y. Song, and L. Xiao, Magnetic properties and phase diagram of quasi-two-dimensional $\text{Na}_2\text{Co}_2\text{TeO}_6$ single crystal under high magnetic field, *J. Phys.: Condens. Matter* **34**, 075801 (2022).

[43] R. Berman, *Thermal Conduction in Solids* (Oxford University Press, Oxford, 1976).

[44] Z. Y. Zhao, X. M. Wang, C. Fan, W. Tao, X. G. Liu, W. P. Ke, F. B. Zhang, X. Zhao, and X. F. Sun, Magnetic phase transitions and magnetoelectric coupling of GdFeO_3 single crystals probed by low-temperature heat transport, *Phys. Rev. B* **83**, 014414 (2011).

[45] See Supplemental Material at <http://link.aps.org/supplemental/10.1103/PhysRevB.107.184423>, which provides characterizations of single-crystal samples and the comparison of thermal conductivity data between Takeda *et al.*'s and ours.

[46] C. Lannert and M. P. A. Fisher, Inelastic Neutron Scattering Signal from Deconfined Spinons in a Fractionalized Antiferromagnet, *Int. J. Mod. Phys. B* **17**, 2821 (2003).

[47] A. Bose, M. Routh, S. Voleti, S. K. Saha, M. Kumar, T. Saha-Dasgupta, and A. Paramekanti, Proximate Dirac spin liquid in the J_1 - J_3 XXZ model for honeycomb cobaltates, [arXiv:2212.13271](https://arxiv.org/abs/2212.13271) (2022).

[48] X. Zhao, Z. Y. Zhao, L. M. Chen, X. Rao, H. L. Che, L. G. Chu, H. D. Zhou, L. S. Ling, J. F. Wang, and X. F. Sun, Frustration-free spatially anisotropic $S = 1$ square-lattice antiferromagnet $\text{Ni}[\text{SC}(\text{NH}_2)_2]_6\text{Br}_2$, *Phys. Rev. B* **99**, 104419 (2019).

[49] J. D. Song, X. M. Wang, Z. Y. Zhao, J. C. Wu, J. Y. Zhao, X. G. Liu, X. Zhao, and X. F. Sun, Low-temperature heat transport of $\text{CuFe}_{1-x}\text{Ga}_x\text{O}_2$ ($x = 0$ -0.12) single crystals, *Phys. Rev. B* **95**, 224419 (2017).

[50] X. M. Wang, C. Fan, Z. Y. Zhao, W. Tao, X. G. Liu, W. P. Ke, X. Zhao, and X. F. Sun, Large magnetothermal conductivity of HoMnO_3 single crystals and its relation to the magnetic-field-induced transitions of magnetic structure, *Phys. Rev. B* **82**, 094405 (2010).

[51] G. Lin, Q. Zhao, G. Li, M. Shu, Y. Ma, J. Jiao, Q. Huang, J. Sheng, A. I. Kolesnikov, L. Li, L. Wi, X. Wang, H. D. Zhou, Z. Liu, and J. Ma, Evidence for field induced quantum spin liquid behavior in a spin-1/2 honeycomb magnet, <https://doi.org/10.21203/rs.3.rs-2034295/v1> (2022).

[52] Y. Ando, J. Takeya, D. L. Sisson, S. G. Doettinger, I. Tanaka, R. S. Feigelson, and A. Kapitulnik, Thermal conductivity of the spin-Peierls compound CuGeO_3 , *Phys. Rev. B* **58**, R2913 (1998).

[53] J. Takeya, I. Tsukada, Y. Ando, T. Masuda, K. Uchinokura, I. Tanaka, R. S. Feigelson, and A. Kapitulnik, Thermal conductivity of pure and Mg-doped CuGeO_3 in the incommensurate phase, *Phys. Rev. B* **63**, 214407 (2001).

[54] Z. Y. Zhao, X. Zhao, H. D. Zhou, F. B. Zhang, Q. J. Li, C. Fan, X. F. Sun, and X. G. Li, Ground state and magnetic phase transitions of orthoferrite DyFeO_3 , *Phys. Rev. B* **89**, 224405 (2014).

[55] N. Li, Q. Huang, A. Brassington, X. Y. Yue, W. J. Chu, S. K. Guang, X. H. Zhou, P. Gao, E. X. Feng, H. B. Cao, E. S. Choi, Y. Sun, Q. J. Li, X. Zhao, H. D. Zhou, and X. F. Sun, Quantum spin state transitions in the spin-1 equilateral triangular lattice antiferromagnet $\text{Na}_2\text{BaNi}(\text{PO}_4)_2$, *Phys. Rev. B* **104**, 104403 (2021).

[56] X. F. Sun, W. Tao, X. M. Wang, and C. Fan, Low-Temperature Heat Transport in the Low-Dimensional Quantum Magnet NiCl_2 - $4\text{SC}(\text{NH}_2)_2$, *Phys. Rev. Lett.* **102**, 167202 (2009).